

Submitted: January 28, 2025

Revised: May 15, 2025

Accepted: May 28, 2025

Elastic deformation and elastic wave velocity in metals (Au, Cu) and interstitial alloy (CuSi) with FCC structure

Q.H. Nguyen^{1,2} , K.V. Tran² , S.G.K. Quach³, Q.T. Doan⁴, N.P.A. Nguyen⁴,
T.S.M. Nguyen¹, D.H. Nguyen⁵, A.T. Tran³ 

¹ Hanoi National University of Education, Hanoi, Vietnam

² Dai Nam University, Hanoi, Vietnam

³ Vietnam National University, Hanoi, Vietnam

⁴ Hanoi-Amsterdam High School for the Gifted, Hanoi, Vietnam

⁵ Mac Dinh Chi High School, Gia Lai, Vietnam

✉ hocnq@hnue.edu.vn

ABSTRACT

A model for face centered cubic binary interstitial alloys and advance the theory of elastic deformation and wave propagation within these alloys using the statistical moment method are presented. The theory extends to include the elastic properties and wave dynamics of pure metals as a subset. The numerical simulations for metals like Au and Cu, as well as the CuSi alloy are conducted. The results obtained for Au and Cu were validated against experimental data and existing calculations. For the CuSi alloy, numerical predictions offer insights that could be confirmed by future experiments.

KEYWORDS

FCC binary interstitial alloy • elastic deformation • elastic wave propagation • statistical moment method

Citation: Nguyen QH, Tran KV, Quach SGK, Doan QT, Nguyen NPA, Nguyen TSM, Nguyen DH, Tran AT. Elastic deformation and elastic wave velocity in metals (Au, Cu) and interstitial alloy (CuSi) with FCC structure. *Materials Physics and Mechanics*. 2025;53(3): 165–176.

http://dx.doi.org/10.18149/MPM.5332025_13

Introduction

Metals and alloys are traditional and popular materials in industry and practical life. There are substitutional alloys and interstitial alloys. In interstitial alloys, the interstitial atoms are usually non-metals such as Si, C, H, Li, etc., which are smaller in size than the main metal atom. Although the interstitial atom concentration is very small, only a few percent, it significantly affects the physical properties of the alloy. Transition metals and their interstitial alloys such as Cu, Au, CuSi, and AuSi are widely applied in superconducting wire fabrication technology [1,2].

Interstitial alloys are crucial in various aspects of human life and have long been a focus for both theoretical and experimental researchers. Investigating the deformation properties of these alloys in relation to temperature, pressure, and interstitial atom concentration is essential for predicting material strength, mechanical stability, diffusion, and other properties [3–5]. AuSi has many functional applications and unusual physical properties.

There are numerous theoretical approaches to studying the elastic deformation of metals and alloys, including the *ab initio* method, molecular dynamics method, the tight-



binding Hamiltonian method, the density functional theory, etc. In the first principles (or *ab initio*) method, the many-electron wavefunction is constructed from the one-electron wavefunctions in a suitable effective potential. The calculations are based primarily on the laws of quantum mechanics and relevant physical constants such as the masses and charges of the nuclei and electrons. *Ab initio* has been widely used in the study of alloy deformations such as the study of the electronic and thermodynamic properties of B₂-eSi interstitial alloy by *ab initio* calculations using *ab initio* plane waves (FPPW) combined with the quasi-harmonic Debye model (QHD) [6], the study of FeH interstitial alloy by *ab initio* combined with DFT (the density functional theory) and GGA (generalized gradient approximation) [7], and the study of FeCrSi alloy by *ab initio* combined with DFT and GGA [8]. *Ab initio* has been used in the study of deformation of metals such as the study of the effect of pressure on the elastic properties of crystalline Au by *ab initio* using local density approximation (LDA) [9] and the study of the elastic modulus of the BCC (body-centered cubic)-Fe [10]. Molecular dynamics (MD) is a method of modeling atoms as a system of classical particles obeying Newtonian mechanics. Newton's second law can be used to write the equation of motion for each atom. Some works using MD to study the deformation of metals and alloys include the thermomechanical properties of CuAu alloy [11], the effect of pressure on the elastic constants of Cu, Ag and Au [12], the thermomechanical properties of some FCC (face centered cubic) transition metals [13], using Morse potential to study the temperature dependence of Young's modulus for metals Ni, Cu, Ag, Au and Al by Zahroh et al. [14]. The tight-coupled Hamiltonian (TB) method [15–17] is simpler, less computationally intensive but can be applied to larger model systems than *ab initio*. Recent studies have used the TB Hamiltonian method to calculate the atomic volumes, elastic constants, bulk moduli, etc. of FCC and HCP (hexagonal close-packed) crystals [17] and to study the structural properties of FCC transition metals [16]. In the density functional theory (DFT), instead of using a multi-electron wave function as in the Hartree-Fock method, the electron density plays a central role [18] and the total energy of the system is a unique function of the electron density. DFT studies of metals and alloys can be mentioned as works by Olsson et al. [19], Psiachos et al. [7] and Lau et al. [20]. In addition to the methods mentioned above, to study the properties of materials, there are other methods such as the modified embedded atom method (MEAM) [21–23], the lattice Green's function method [24], the machine learning method (MLM) [25], harmonic theory [26] and quasi-harmonic theory [27], etc. From the methods presented above, we see that most of the methods for studying the deformation of metal and alloy crystals are approximate methods, not mentioning the influence of pressure on the deformation processes of the object, not considering the dependence of the deformation quantities depending on the concentration of substitutional and interstitial atoms. The results of theoretical methods for studying deformation are mostly for metals and are limited for alloys. Some results obtained from theoretical methods are not really consistent with experiments.

For example, the interaction of impurity atoms of light elements with vacancies and vacancy clusters in FCC metals was studied by MD of Poletaev et al. [28]. Among theoretical methods in studying mechanical and thermodynamic properties of metals and alloys, the statistical moment method (SMM) has significant contributions [29]. SMM is a contemporary approach in statistical physics used to examine the structure,

thermodynamic properties, elasticity, diffusion, phase transitions of metals, alloys, semiconductors, inert gases, oxides with BCC, FCC and HCP structures. SMM has been particularly applied to the thermodynamic study of cubic interstitial alloys [30–35]. Recently, the SMM has been successfully applied in the study of thermomechanical properties of multicomponent materials with complex structures such as HCP metals of Hoc et al. [36,37], ternary and binary interstitial alloys of Hoc et al. [34,38,39], perovskite-structured alloys of Hoc et al. [40–42].

There are many studies on classical wave propagation in complex materials with periodic structure [43–46]. Some work has been extended to the study of sound waves and elastic waves in other periodic media. Most of the research on this problem is based on the calculations of the plane wave method [47–51]. The planar wave method has proved to be quite effective in studying many types of periodic complex structures but is less effective for disordered chaotic systems. Multiple-scattering theory (MST) method [52,53] is based on electronic band structure calculations. The equations of motion of the particles are built in an elastic body [54]. Some works such as the work of Grechka et al. [55] refer to the propagation of sound waves in an anisotropic medium. Mozhaev [56] showed its applicability to two- and three-partial surface acoustic waves in crystals. Additionally, Nayfeh and Chimenti [57] extend the analysis to free wave propagation in a general anisotropic plate, presenting numerical results for special cases.

In this paper, we examine the elastic deformation and wave propagation in FC binary interstitial alloys under pressure using the SMM. The next section will detail the theory and methodology and numerical results.

Theory and Methodology

Our model of FCC interstitial alloy AB assumes that the concentration of interstitial atoms B is very small compared to the concentration of main metal atoms A. In this model, atoms B are located at the body center, atoms A_1 are at the face centers, and atoms A_2 are at the vertices of the cubic unit cells [30–35].

To investigate the elastic properties of alloy AB using SMM, we first calculate the mean nearest neighbor distance between two atoms A in the alloy using the following equations [31,32,35]:

$$\begin{aligned}
 \overline{r_{1A}(P,T)} &= \overline{r_{01A}(P,0)} + \overline{y(P,T)}, \quad \overline{r_{01A}(P,0)} = (1 - c_B)r_{01A}(P,0) + c_B r_{01A}'(P,0), \\
 \overline{y(P,T)} &= \sum_X c_X y_X(P,T), \quad r_{01A}'(P,0) = \sqrt{3}r_{01B}(P,0), \\
 r_{1B}(P,T) &= r_{01B}(P,0) + y_{A_1}(P,T), \quad r_{1A}(P,T) = r_{01A}(P,0) + y_A(P,T), \\
 r_{1A_1}(P,T) &= r_{1B}(P,T), \quad r_{1A_2}(P,T) = r_{01A_2}(P,0) + y_B(P,T), \\
 y_X(P,T) &= \sqrt{\frac{2y_X(P,0)\theta^2}{3k_X^3(P,0)}} A_X(P,T), \quad A_X(P,T) = a_{1X}(P,T) + \sum_{i=2}^6 \left(\frac{y_X(P,0)\theta}{k_X^2(P,0)} \right)^i a_{iX}(P,T), \\
 Z_X &\equiv x_X \coth x_X, \quad x_X = \frac{\hbar}{2\theta} \sqrt{\frac{k_X}{m_X}}, \\
 a_{1X} &= 1 + \frac{1}{2}Z_X, \quad a_{2X} = \frac{13}{3} + \frac{47}{6}Z_X + \frac{23}{6}Z_X^2 + \frac{1}{2}Z_X^3, \\
 a_{3X} &= -\left(\frac{25}{3} + \frac{121}{6}Z_X + \frac{50}{3}Z_X^2 + \frac{16}{3}Z_X^3 + \frac{1}{2}Z_X^4 \right), \\
 a_{4X} &= \frac{43}{3} + \frac{93}{2}Z_X + \frac{169}{3}Z_X^2 + \frac{83}{3}Z_X^3 + \frac{22}{3}Z_X^4 + \frac{1}{2}Z_X^5,
 \end{aligned} \tag{1}$$

$$a_{5X} = - \left(\frac{103}{3} + \frac{749}{6} Z_X + \frac{363}{2} Z_X^2 + \frac{391}{3} Z_X^3 + \frac{148}{3} Z_X^4 + \frac{53}{6} Z_X^5 + \frac{1}{2} Z_X^6 \right),$$

$$a_{6X} = 65 + \frac{561}{2} Z_X + \frac{1489}{3} Z_X^2 + \frac{927}{2} Z_X^3 + \frac{733}{3} Z_X^4 + \frac{145}{2} Z_X^5 + \frac{31}{3} Z_X^6 + \frac{1}{2} Z_X^7.$$

Here, $\overline{r_{1A}(P,T)} \equiv a_{1A}(P,T)$ and $\overline{r_{01A}(P,0)} \equiv a_{01A}(P,0)$ denote the mean nearest neighbor distances between two atoms A in the alloy under pressure P and temperature T , and under pressure P and temperature $T = 0$ K, respectively. The mean displacement of atom A from its equilibrium position in the alloy is indicated by $\overline{y}(P,T)$. The nearest neighbor distance between two atoms A in the pure metal is labeled $r_{01A}(P,0)$. The distance between two atoms A in the region containing the interstitial atom B is denoted by $r'_{01A}(P,0)$. The displacement of an atom X (where X can be A, A₁, A₂, B) within the alloy is represented by $y_X(P,T)$. The nearest neighbor distances between two atoms A in the pure metal or between atom X and other atoms in the alloy are represented by $r_{1X}(P,T)$ and $r_{01X}(P,0)$.

The value $r_{01X}(P,0)$ is derived either from the condition of minimum u_{0X} or from the equation of state, as detailed in [30,32,33]:

$$Pv_{0X} = - r_{01X} \left(\frac{1}{6} \frac{\partial u_{0X}}{\partial r_{01X}} + \frac{\hbar \omega_{0X}}{4k_X} \frac{\partial k_X}{\partial r_{01X}} \right), \quad (2)$$

where $r_{01X} \equiv r_{01X}(P,0)$, $v_{0X} = \frac{r_{01X}^3}{\sqrt{2}}$, $\omega_{0X} = \sqrt{\frac{k_X(P,0)}{m_X}}$, $c_X = \frac{N_X}{N}$, $N = N_A + N_{A_1} + N_{A_2} + N_B$, $\theta = k_B T$, k_B represents the Boltzmann constant, \hbar is the Planck constant. The symbol m_X denotes the mass of atom X. The terms u_{0X} , k_X , γ_{1X} , γ_{2X} and γ_X correspond to the cohesive energy and crystal parameters of atom X within the metal A or the alloy AB, as detailed in [30,32,33]:

$$u_{0X} = \frac{1}{2} \sum_{i=1}^{n_i} \varphi_{i0},$$

$$k_X = \frac{1}{2} \sum_{i=1}^{n_i} \left(\frac{\partial^2 \varphi_{i0}}{\partial u_{i\beta}^2} \right)_{eq} = m_X \omega_X^2, \gamma_X = 4(\gamma_{1X} + \gamma_{2X}), \quad (3)$$

$$\gamma_{1X} = \frac{1}{48} \sum_{i=1}^{n_i} \left(\frac{\partial^4 \varphi_{i0}}{\partial u_{i\beta}^4} \right)_{eq}, \gamma_{2X} = \frac{6}{48} \sum_{i=1}^{n_i} \left(\frac{\partial^4 \varphi_{i0}}{\partial u_{i\alpha}^2 \partial u_{i\beta}^2} \right)_{eq},$$

where $u_{i\beta}(\beta = x, y, z)$ represents the displacement of the i^{th} particle from its equilibrium position in the direction β , φ_{i0} indicates the interaction potential between the 0th particle and the i^{th} particle, and (...)eq denotes the value of these parameters at equilibrium. The number of atoms in n_i coordination sphere is indicated by n_i , $\alpha, \beta = x, y, z, \alpha \neq \beta$.

The Helmholtz free energy of the alloy AB is expressed as follows [29–33,35]:

$$\Psi_{AB} = N\psi_{AB} = N(\sum_X c_X \psi_X - TS_c^{AB}),$$

$$\Psi_X = N\psi_X = U_{0X} + \psi_{0X} + 3N \left\{ \frac{\theta^2}{k_X^2} \left[\gamma_{2X} Z_X^2 - \frac{2\gamma_{1X}}{3} \left(1 + \frac{Z_X}{2} \right) \right] + \right.$$

$$\left. + \frac{2\theta^3}{k_X^4} \left[\frac{4}{3} \gamma_{2X}^2 Z_X \left(1 + \frac{Z_X}{2} \right) - 2(\gamma_{1X}^2 + 2\gamma_{1X}\gamma_{2X}) \left(1 + \frac{Z_X}{2} \right) (1 + Z_X) \right] \right\},$$

$$\psi_{0X} = 3N\theta [x_X + \ln(1 - e^{-2x_X})], \quad (4)$$

where $c_A = 1 - 15c_B$, $c_{A_1} = 6c_B$, $c_{A_2} = 8c_B$ and S_c^{AB} is the configurational entropy of the alloy AB.

Young modulus of the alloy AB is given by [31,33,34,36]:

$$E_{YAB} = E_{YA} \frac{\sum_X c_X \frac{\partial^2 \psi_X}{\partial \varepsilon^2}}{\frac{\partial^2 \psi_A}{\partial \varepsilon^2}}, E_A = \frac{1}{\pi r_{1A} B_{1A}}, B_{1A} = \frac{1}{k_A} \left[1 + \frac{2\gamma_A^2 \theta^2}{k_A^4} \left(1 + \frac{1}{2} Z_A \right) (1 + Z_A) \right], \quad (5)$$

$$\frac{1}{3N} \frac{\partial^2 \psi_X}{\partial \varepsilon^2} = \left\{ \frac{2}{3} \frac{\partial^2 u_{0X}}{\partial r_{1X}^2} + \frac{\hbar \omega_X}{k_X} \left[\frac{\partial^2 k_X}{\partial r_{1X}^2} - \frac{1}{2k_X} \frac{\partial k_X}{\partial r_{1X}} \right] \right\} r_{01X}^2 + \left(\frac{\partial u_{0X}}{\partial r_{1X}} + \frac{3\hbar \omega_X \coth x_X}{2k_X} \frac{\partial k_X}{\partial r_{1X}} \right) r_{01X},$$

where E_{YA} is Young's modulus of the pure metal A and ε represents the strain of the alloy AB.

The bulk modulus K_{AB} , shear modulus G_{AB} , elastic constants C_{11AB} , C_{12AB} , C_{44AB} , Poisson's ratio ν_{AB} , longitudinal wave velocity V_{lAB} and transverse wave velocity V_{tAB} are calculated by Hoc et al. [30,32,33,35]:

$$K_{AB} = \frac{E_{YAB}}{3(1-2\nu_{AB})}, \quad (6)$$

$$G_{AB} = \frac{E_{YAB}}{2(1+\nu_{AB})}, \quad (7)$$

$$C_{11AB} = \frac{E_{YAB}(1-\nu_{AB})}{(1+\nu_{AB})(1-2\nu_{AB})}, C_{12AB} = \frac{E_{YAB}\nu_{AB}}{(1+\nu_{AB})(1-2\nu_{AB})}, C_{44AB} = \frac{E_{YAB}}{2(1+\nu_{AB})}, \quad (8)$$

$$\nu_{AB} = c_A \nu_A + c_B \nu_B \approx \nu_A, \quad (9)$$

$$V_{lAB} = \sqrt{\frac{2C_{44AB} + C_{12AB}}{\rho_{AB}}}, V_{tAB} = \sqrt{\frac{C_{44AB}}{\rho_{AB}}}, \quad (10)$$

where ν_A and ν_B respectively are the Poisson ratios of materials A and B, $\rho_{AB} = \frac{m_{AB}}{V_{AB}} \approx \rho_A$, $V_{AB} = N\nu_{AB}$, ρ_{AB} and ρ_A denote the densities of materials A and AB, respectively while V_{AB} represents the volume of alloy AB.

When the concentration of interstitial atoms is zero, the characteristic quantities for elastic deformation and elastic wave propagation of the primary metal A can be ascertained. For Au, Cu, and CuSi, we utilize the Mie-Lennard-Jones (MLJ) potential as follows Magomedov [58,59]:

$$\varphi(r) = \frac{D}{n-m} \left[m \left(\frac{r_0}{r} \right)^n - n \left(\frac{r_0}{r} \right)^m \right]. \quad (11)$$

The parameters D , r_0 , n , m , the Poisson's ratio ν and the density ρ are listed in Table 1.

Table 1. Potential parameters, Poisson ratio ν and density ρ [58–60]

Interaction	m	n	D/k_B , K	r_0 , 10^{-10} m	ν	ρ , g/cm ³
Au-Au	5.5	10.5	4683	2.8751	0.39	19.283
Cu-Cu	5.5	11	3401.1	2.5487	0.37	8.932
Si-Si	6	12	32701.7	2.295	0.28	2.329

The Cu-Si interaction is also described using the MLJ n-m potential:

$$\varphi(r) = \frac{\bar{D}}{\bar{n}-\bar{m}} \left[\bar{m} \left(\frac{r_0}{r} \right)^{\bar{n}} - \bar{n} \left(\frac{r_0}{r} \right)^{\bar{m}} \right], \quad (12)$$

where

$$\bar{D}_{Cu-Si} = \sqrt{D_{Cu-Cu} D_{Si-Si}}, \bar{r}_{0Cu-Si} = \frac{1}{2} (r_{0Cu-Cu} + r_{0Si-Si}), \quad (13)$$

where \bar{n} and \bar{m} are empirically determined [61]. Therefore, $\bar{D}_{Cu-Si}/k_B = 10546.2$ K, $\bar{r}_{0Cu-Si} = 2.4218 \times 10^{-10}$ m, and we empirically choose $\bar{n} = 1.29$, $\bar{m} = 9.92$ by fitting the theoretical result with the experimental data of Santra et al. [2].

The numerical calculations for Au, Cu and CuSi are placed below. The calculated results for the elastic moduli E_Y and K , the volume ratio V/V_0 (where V is the volume at pressure P and V_0 is the volume at $P = 0$), the elastic constant C_{44} and the longitudinal wave velocity V_l for metals Au and Cu are summarized in Table 2 and illustrated in Figs. 1–6.

Table 2. G(P,T) for Cu from SMM calculations, other calculations and experiments

P , GPa	T , K	G , GPa SMM	G , GPa Expt. [62]	G , GPa Calc. [62]	$\delta_{SMM-Expt. [62]}$, %	$\delta_{Calc. [31]-Expt. [62]}$, %
12.1	346	5.94	6.28	5.95	5.7	5.5
12.5	348	6.00	5.90	5.99	1.7	1.5
23.2	418	7.50	7.55	7.14	0.7	5.7

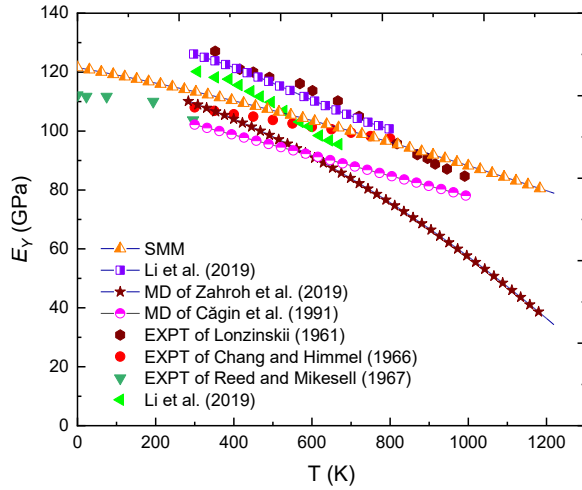


Fig. 1. The temperature dependence of Young modulus E_Y for Cu at $P = 0$ using SMM calculations, other calculations [13,63,64] and experiments [64–67]

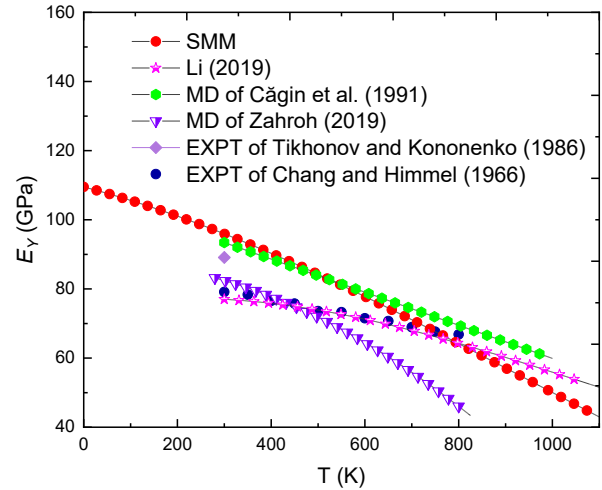


Fig. 2. The temperature dependence of Young modulus E_Y for Au at $P = 0$ using SMM calculations, other calculations [13,14,66] and experiments [65,68]

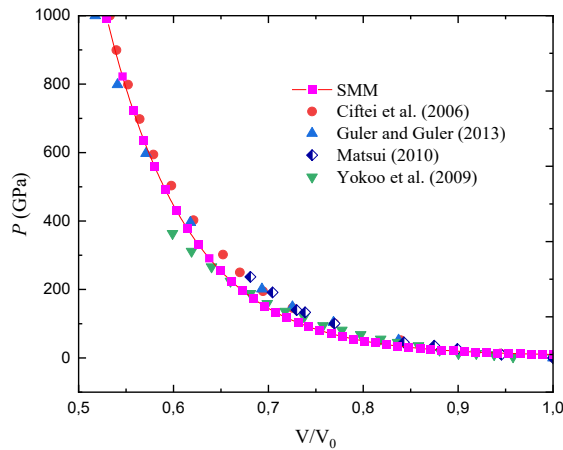


Fig. 3. The pressure dependence of volume ratio V/V_0 for Au at $T = 300\text{K}$ using SMM calculations and other calculations [21,69–71]

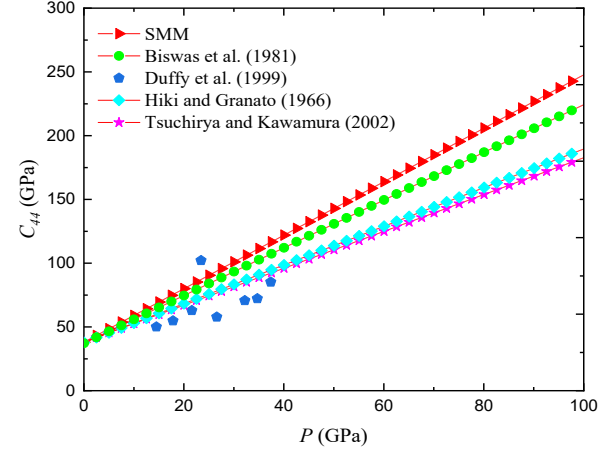


Fig. 4. The pressure dependence of elastic constant C_{44} for Au at $T = 300\text{K}$ using SMM calculations and experiments [3,9,72,73]

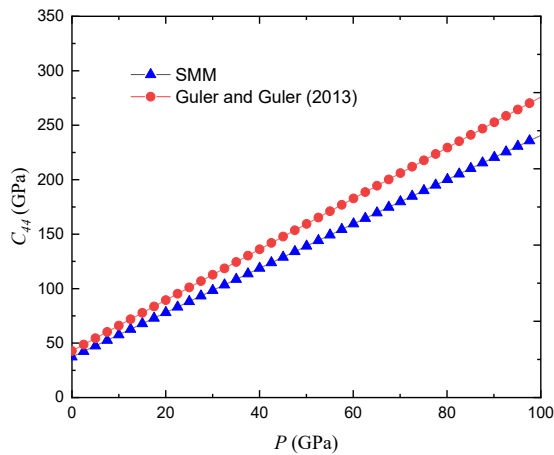


Fig. 5. The pressure dependence of elastic constant C_{44} for Au at $T = 300\text{K}$ using SMM calculations and other calculations [21]

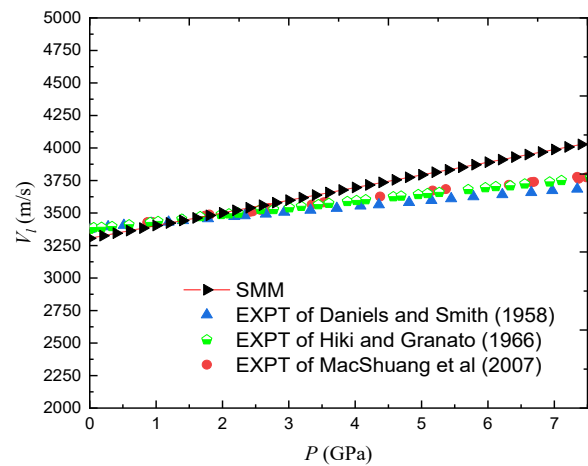


Fig. 6. The pressure dependence of longitudinal wave velocity V_l for Au at $T = 300\text{K}$ using SMM calculations and experiments [73–75]

In Table 2, we compare the shear modulus G of Cu calculated by the SMM with other theoretical calculations and experimental data from Peng et al. [62]. The SMM calculations are in good agreement with both the theoretical and experimental results of Peng et al. [62] with an overall error of 5.7 %. Notably, at $P = 23.2$ GPa, the discrepancy between the SMM calculations and experimental results is only 0.7 %, whereas the error between Peng et al. calculations [62] and experiments is 5.7 %.

Figure 1 shows the temperature dependence of Young's modulus E_Y for Cu at $P = 0$ in the range from 0 to 1200 K. The SMM calculations are in good agreement with calculations of Căgin et al. [13], Li et al. [63], Zahroh et al. [14] and experiments of Lonzinskii [64], Chang and Himmel [65], Reed and Mikesell [66], Joshi and Bhatnagar [67]. Figure 2 illustrates the temperature dependence of Young's modulus E_Y for Au at $P = 0$ in the range from 0 to 1100 K. The SMM calculations are in good agreement with calculations of Căgin et al. [13], Li et al. [63], Zahroh et al. [14] as well as experiments of Chang and Himmel [65], Tikhonov and Kononenko [68]. Figure 3 shows the pressure dependence of volume ratio V/V_0 for Au at $T = 300$ K in the range from 0 to 1000 GPa. The SMM calculations are in excellent agreement with other calculations of Ciftci et al. [69], Yokoo et al. [70], Matsui [71] and Guler and Guler [21]. Figure 4 illustrates the pressure dependence of elastic constant C_{44} for Au at $T = 300$ K in the range from 0 to 100 GPa. SMM calculations are compared with experimental data from Biswas et al. [72], Hiki and Granato [73], Duffy et al. [3], Tsuchiya and Kawamura [9]. The SMM calculations align more closely with experimental data in the range from 0 to 30 GPa than in the range from 30 to 100 GPa. Most SMM calculations are higher than the experimental values with the discrepancy increasing at higher pressures. This difference is likely due to the influence of defects such as vacancies on the metal's volume at high pressures, which is not accounted for in our model. Figure 5 presents the pressure dependence of the elastic constant C_{44} for Au at $T = 300$ K in the range from 0 to 100 GPa calculated by SMM and other calculations of Guler and Guler [21]. The observations and comments for this figure are similar to those for Fig. 4. The pressure dependence of longitudinal wave velocity V_ℓ for Au at $T = 300$ K in the range from 0 to 7.5 GPa is shown in Fig. 6. Here there is a good agreement between SMM calculations and experiments of Hiki and Granato [73], Daniels and Smith [74], Mao Shuang et al. [75]. The agreement between SMM calculations and experiments in the range from 0 to 2 GPa is better than in the range from 2 to 7.5 GPa.

The analysis above indicates that SMM calculations for metals Au and Cu are in very good agreement with experimental data and other calculations. In many cases, our SMM calculations are closer to the experimental values in comparison with other calculations. This provides a strong foundation for our subsequent calculations for the interstitial alloy CuSi.

The SMM calculations for elastic deformation quantities of CuSi are shown in Figs. 7 and 8. Figure 7 illustrates the silicon atom concentration dependence of Young's modulus E_Y for CuSi at $T = 300$ K and $P = 0$ in the range of silicon atom concentration from 0 to 5 %. These SMM calculations are compared with experimental data from Ledbetter and Naimon [76] and Santra et al. [2]. As silicon concentration increases, E_Y decreases, which is consistent with experiments of Santra et al. [2]. The closest alignment between our calculations and experimental data is at a silicon concentration of 4 %. Figure 8 shows the temperature and pressure dependence of Young's modulus E_Y for CuSi at silicon

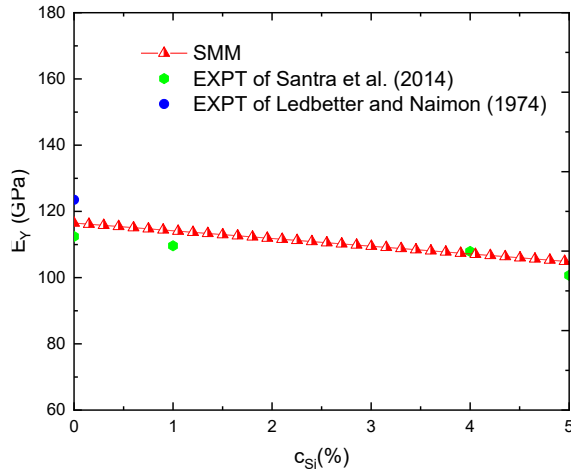


Fig. 7. The silicon atom concentration dependence of Young's modulus E_Y for CuSi at $T = 300$ K and $P = 0$ using SMM calculations and experiments [2,76]

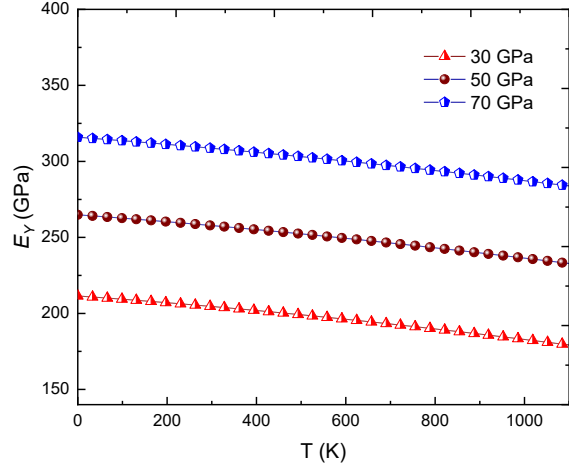


Fig. 8. The temperature and pressure dependence of Young's modulus E_Y for CuSi at silicon concentration $c_{Si} = 1$ % using SMM calculations

concentration $c_{Si} = 1$ % in the temperature range from 0 to 1100 K and the pressure range from 30 to 70 GPa using SMM calculations. Our SMM calculations demonstrate that Young's modulus for CuSi decreases with increasing temperature and increases with increasing pressure.

Young's modulus E_Y of CuSi exhibits a decline with increasing temperature T . For CuSi with a silicon concentration of 3 % and at $P = 0$, E_Y drops from 114.89 to 93.45 GPa as T rises from 0 to 1100 K. This is because the kinetic energy of the atoms increases with temperature, causing the lattice constants to expand, and consequently, E_Y , K , G , C_{11} , C_{12} , C_{44} , V_ℓ and V_t all decrease. Conversely, E_Y increases with pressure P . For CuSi with 1 % silicon at $T = 300$ K, E_Y rises from 114.28 to 308.58 GPa as P increases from 0 to 70 GPa. This is due to the compressive force acting on the material, which reduces the lattice constant and results in increases in E_Y , K , G , C_{11} , C_{12} , C_{44} , V_ℓ and V_t . Additionally, E_Y decreases as the concentration of interstitial silicon atoms increases. Our SMM calculations align well with the experimental data from Santra et al. [2]. As explained by this group, when the crystal lattice of Cu is supplemented with Si, the lattice constants increase.





Increases according to a linear law. As a result, the interactions between the particles in the crystal lattice weaken and E_Y , K , G , C_{11} , C_{12} , C_{44} , V_ℓ and V_t decrease. This rule is also consistent with experiments of Smith and Burns [77], in which, when c_{Si} increases from 0 to 4 %, C_{44} of CuSi decreases from 75.6 to 75.5 GPa.

Conclusions

The new contribution of the paper is the development of statistical moment method (SMM) in studying the elastic deformation properties and elastic wave velocity of interstitial alloy materials with face-centered cubic (FCC) structure. By applying SMM, the paper derives the analytical expression of Helmholtz free energy, the average nearest neighbor distance between two main metal atoms, characteristic elastic deformation and elastic wave quantities such as Young's modulus, bulk compressive modulus, shear modulus, elastic constants, longitudinal wave velocity and transverse wave velocity of

binary interstitial alloys with FCC structure. The elastic deformation and elastic wave quantities of the main metal in the interstitial alloy are a special case when the interstitial atom concentration is zero. The numerical calculation results of SMM using Mie-Lennard-Jones (n-m) interaction potential, coordination sphere method, Maple and Origin softwares for Au, Cu metals are in good agreement with the experimental results and other calculation results. The numerical results for CuSi interstitial alloys are new and predictive, providing guidance for experiments. The studied temperature range is from 0 to 1200 K, the studied pressure range is from 0 to 1000 GPa and the interstitial atomic concentration range is from 0 to 5 %.

CRediT authorship contribution statement

Nguyen Quang Hoc  **Sc**: conceptualization, methodology, validation, investigation, project management, supervisor, writing - original draft preparation, data curation, writing-review and editing; **Tran Ky Vi**  **Sc**, **Quach Si Gia Khoa**, **Doan Quang Tuan**, **Nguyen Ngoc Phuong Anh**, **Nguyen Thi Sao Mai**, **Nguyen Duc Hien** **Sc**, **Tran Anh Tuan**  **Sc** : investigation, data analysis, resource, software, visualization, writing—original draft preparation.

Conflict of interest

The authors declare that they have no conflict of interest.

References

1. Nyilas RD, Frank S, Spolenak R. Revealing plastic deformation mechanisms in polycrystalline thin films with synchrotron XRD. *JOM: The Journal of Minerals, Metals and Materials Society*. 2010;62: 44–51.
2. Santra S, Dong H, Laurila T, Paul A. Role of different factors affecting interdiffusion in Cu(Ga) and Cu(Si) solid solutions. *Proceedings of Royal Society A*. 2014;470(2161): 20130464.
3. Duffy TS, Shen G, Heinz DL, Shu J, Ma Y, Mao HK, Hemley RJ, Singh AK. Lattice strains in gold and rhenium under nonhydrostatic compression to 37 GPa. *Physical Review B*. 1999;60(22): 15063–15073.
4. Esfahani MN, Jabbari M. Molecular dynamics simulations of deformation mechanisms in the mechanical response of nanoporous gold. *Materials*. 2020;13(9): 2071.
5. Singh BN, Huang X, Tähtinen S, Moilanen P, Jacquet P, Dekeyser J. *Final report on in-reactor uniaxial tensile deformation of pure iron and Fe-Cr alloy*. Roskilde: Risø National Laboratory; 2007.
6. Zhao KM, Jiang G, Wang L. Electronic and thermodynamic properties of B₂-FeSi from first-principles. *Physica B Condensed Matter*. 2011;406(3): 363–367.
7. Psiachos D, Hammerschmidt T, Drautz R. Ab initio study of the modification of elastic properties of α -iron by hydrostatic strain and by hydrogen interstitials. *Acta Materialia*. 2011;59(11): 4255–4263.
8. Zhang J, Su C, Liu Y. First-principles study of bcc FeCrSi binary and ternary random alloys from special quasi-random structure. *Physica B: Condensed Matter*. 2020;586: 412085.
9. Tsuchiya T, Kawamura K. Ab initio study of pressure effect on elastic properties of crystalline Au. *Journal of Chemical Physics*. 2002;116(5): 2121–2124.
10. Zhang H, Punkkinen MPI, Johansson BS, Vitos L. Theoretical elastic moduli of ferromagnetic bcc Fe alloys. *Journal of Physics: Condensed Matter*. 2010;22(27): 275402.
11. Kart HH, Tomak M, Çağın T. Thermal and mechanical properties of Cu–Au intermetallic alloys. *Modelling and Simulation in Materials Science and Engineering*. 2005;13(5): 657.
12. Ciftci YO, Colakoglu K, Kazanc S, Ozgen S. The effect of pressure on the elastic constants of Cu, Ag and Au: a molecular dynamics study. *Open Physics*. 2006;4(4): 472–480.

13. Çağın T, Dereli, Uludoğan, Tomak M. Thermal and mechanical properties of some fcc transition metals. *Physical Review B*. 1985;59(5): 3468–3473.
14. Zahroh FF, Sugihartono I, Safitri ED. Young's modulus calculation of some metals using molecular dynamics method based on the Morse potential. *Computational and Experimental Research in Materials and Renewable Energy (CERiMRE)*. 2019;2(1): 19–34.
15. Mehl MJ, Papaconstantopoulos DA, Kiossis N, Herbranson M. Tight-binding study of stacking fault energies and the Rice criterion of ductility in the fcc metals. *Physical Review B*. 2000;61(7): 4894–4897.
16. Rosato V, Guillope M, Legrand B. Thermodynamical and structural properties of fcc transition metals using a simple tight-binding model. *Philosophical Magazine A*. 1989;59(2): 321–336.
17. Vocadlo L, Price GD, Wood IG. Crystal structure, compressibility and possible phase transitions in – FeSi studied by first-principles pseudopotential calculations. *Acta Crystallographica Section B: Structural Science, Crystal Engineering and Materials*. 1999;55: 484–493.
18. Kohn W. Electronic structure of matter-wave functions and density functionals. *Review Modern Physics*. 1999;71(5): 1253–1266.
19. Olsson P, Abrikosov IA, Vitos L, Wallenius J. Ab initio formation energies of Fe–Cr alloys. *Journal of Nuclear Materials*. 2003;321: 84–90.
20. Lau TT, Först CJ, Lin X, Gale JD, Yip S, Vliet VKJ. Many-body potential for point defect clusters in Fe–C alloys. *Physical Review Letters*. 2007;98(21): 215501.
21. Güler E, Güler M. Geometry optimization calculations for the elasticity of gold at high pressure. *Advances in Materials Science and Engineering*. 2013;2013: 525673.
22. Lee B-J, Jang J-W. A modified embedded-atom method interatomic potential for the Fe–H system. *Acta Materialia*. 2007;55: 6779–6788.
23. Liyanage LSI, Kim SG, Houze J, Kim S, Tschopp MA, Baskes MJ, Horstemeyer MF. Structural, elastic and thermal properties of cementite (Fe₃C) calculated using a modified embedded atom method. *Physical Review B*. 2014;89: 094102.
24. Masuda-Jindo K, Hung VV. Atomistic study of fracture of crystalline materials by lattice Green's function method: Effects of anharmonicity of lattice vibration. *Journal of the Physical Society of Japan*. 2004;73(5): 1205–1215.
25. Mazhnik E, Oganov AR. Application of machine learning methods to predicting new superhard materials. *Journal of Applied Physics*. 2020;128(7): 075102.
26. Born M, Oppenheimer R. Zur quantentheorie der Molekeln. *Annalen der Physik*. 1927;389(20): 457–484.
27. Mie G. Zur kinetischen theorie der einatomigen Körper. *Annalen der Physik*. 2006;316(8): 657–697.
28. Poletaev GM, Zorya IV, Rakitin RI, Iliina MA, Starostenkov MD. Interaction of impurity atoms of light elements with vacancies and vacancy clusters in FCC metals. *Materials Physics and Mechanics*. 2020;44(1): 26–33.
29. Tang N, Hung VV. Investigation of the thermodynamic properties of anharmonic crystals by the momentum method, I. General results for face-centered cubic crystals. *Physica Status Solidi B-Basic Solid State Physics*. 1988;149(2): 511–519.
30. Nguyen HQ, Bui DT, Nguyen DH, Coman GI. Study of nonlinear deformation of FCC–AuCuSi under pressure by the statistical moment method. *Advances in Materials Science and Engineering*. 2021;2021(5–6): 1–11.
31. Nguyen HQ, Nguyen HT, Coman GI, Cuong TD, Hong VL. Thermodynamic property of FCC interstitial alloy AuSi with defects. *IOP Conference Series: Materials Science and Engineering*. 2019;485(1): 012018.
32. Nguyen HQ, Bui DT, Nguyen DH. Stress-strain curve of FCC interstitial alloy AuSi under pressure. *Romanian Journal of Physics*. 2020;65(5–6): 608.
33. Nguyen HQ, Nguyen DH. Elastic deformation of alloy AuSi with FCC structure under pressure. *HNUE Journal of Science, Natural Science*. 2018;63(6): 74–83.
34. Hoc NQ, Tinh BD, Hien ND, Coman G. Nonlinear deformation of BCC metal Fe and BCC interstitial alloy FeSi: Dependence on temperature, pressure and silicon concentration. *Materials Physics and Mechanics*. 2021;47(3): 501–513.
35. Nguyen HQ, Bui DT, Nguyen DH, Le TD. Elastic deformation of binary and ternary interstitial alloys with FCC structure and zero pressure: Dependence on temperature, concentration of substitution atoms and concentration of interstitial atoms. *HNUE Journal of Science, Mathematical and. Physical Sciences*. 2016;61(7): 47–57.
36. Nguyen HQ, Phan MH, Nguyen ML, Dao NH, Pham TT, Nguyen MV, Vu CC, Nguyen SM. Study on elastic deformation and thermodynamic properties of metals Mg, Zn, Dy, Er and Gd with HCP structure by statistical moment method: Dependences on temperature and pressure. *Modern Physical Lettes B*. 2023;38(4): 2350241.
37. Nguyen HQ, Nguyen TD, Dat HX, Lam LT. Theoretical predictions of thermodynamic properties, elastic deformation, HCP–FCC structural phase transition and melting of iron at high temperatures up to 18000 K and high pressures up to 4000 GPa. *Physics Letters A*. 2025;535: 130281.

38. Nguyen HQ, Nguyen DH. Study on thermodynamic and elastic properties of B₂-FeSi under pressure by statistical moment method according to models of interstitial and substitutional alloys. *High Temperatures-High Pressures*. 2022;51(4): 295.
39. Nguyen HQ, Nguyen DH, Tran VK. Elastic deformation and elastic wave velocity of iron and its binary interstitial alloys: Temperature, pressure and interstitial atom concentration dependences. *Physica B Condensed Matter*. 2022;644(5): 414134.
40. Nguyen HQ, Than TN, Ngo NT, Bui LN, Nguyen TN, Le LT. Toward better understanding of anharmonic structural, thermodynamic and elastic properties of CaSiO₃ perovskite under extreme condition investigated via statistical moment method. *Materialia*. 2024;34: 102105.
41. Nguyen HQ, Nguyen DT, Thang NN, Nguyen VH, Le LT. Melting curves of MgSiO₃ and CaSiO₃ perovskites with cubic structure at extreme condition. *Journal of Applied Physics*. 2024;136: 045103.
42. Nguyen HQ, Nguyen QN, Dao MT, Tran VC, Lai TT, Le TT, Nguyen AT. Thermodynamic properties of perovskite MgSiO₃ with cubic structure under extreme conditions. *The European Physical Journal B*. 2024;97: 167.
43. Ho KM, Chan CT, Soukoulis CM. Existence of a photonic gap in periodic dielectric structures. *Physical Review Letters*. 1990;65(25): 3152.
44. Yablonovitch E. Inhibited spontaneous emission in solid-state physics and electronics. *Physical Review Letters*. 1987;58(20): 2059.
45. Yablonovitch E, Gmitter TJ. Photonic band structure: The face-centered-cubic case. *Physical Review Letters*. 1989;63(18):1950.
46. Wang X, Zhang XG, Yu Q, Harmon BN. Multiple-scattering theory for electromagnetic waves. *Physical Review B*. 1993;47(8): 4161.
47. Economou EN, Sigalas M. Stop bands for elastic waves in periodic composite materials. *Journal of Acoustical Society of American*. 1994;95: 1734–1740.
48. Klironomos AD, Economou EN. Elastic wave band gaps and single scattering. *Solid State Communications*. 1998;105(5): 327–332.
49. Kushwaha MS, Halevi P, Martinez G, Dobrzynski L, Djafari-Rouhani B. Theory of acoustic band structure of periodic elastic composites. *Physical Review B*. 1994;49(4): 2313.
50. Montero de Espinosa FR, Jimenez E, Torres M. Ultrasonic band gap in a periodic two-dimensional composite. *Physical Review Letters*. 1998;80(6): 1208.
51. Sanchez-Perez JV, Caballero D, Martinez-Sala R, Rubio C, Sanchez-Dehesa J, Meseguer F, Llinares J, Galvez F. Sound attenuation by a two-dimensional array of rigid cylinders. *Physical Review Letters*. 1998;80(24): 5325.
52. Butler WH, Gonis A, Zhang X-G. Multiple-scattering theory for space-filling cell potentials. *Physical Review B*. 1992;45(20): 11527.
53. Zhang X-G, Butler WH. Multiple-scattering theory with a truncated basis set. *Physical Review B*. 1992;46(12): 7433.
54. Bich DH. *Elastic theory*. Hanoi: VNU Publishing House; 2001.
55. Grechka V, Zhang L, Rector JW. Shear waves in acoustic anisotropic media. *Geophysics*. 2004;69(2): 576-582.
56. Mozhaev VG. Some New Ideas in the Theory of Surface Acoustic Waves in Anisotropic Media. In: Parker DF, England AH. (eds.) *IUTAM Symposium on Anisotropy, Inhomogeneity and Nonlinearity in Solid Mechanics. Solid Mechanics and Its Applications*. Dordrecht: Springer; 1995. p.455–462.
57. Nayfeh AH, Chimenti DE. Propagation of guided waves in fluid-coupled plates of fiber-reinforced composite. *Journal of Acoustical Society of American*. 1988;83: 1736–1743.
58. Magomedov MN. On calculating the Debye temperature and the Gruneisen parameter. *Journal of Chemical Physics*. 1987;61(4): 1003–1009. (In Russian)
59. Magomedov MN. The calculation of the parameters of the Mie-Lennard-Jones potential. *High Temperature*. 2006;44(4): 513–529.
60. Lide DR. *CRC Handbook of Chemistry and Physics*. 86th ed. Boca Raton: CRC Press; 2005.
61. Good RJ, Hope CJ. New combining rule for intermolecular distances in intermolecular potential functions. *Journal of Chemical Physics*. 1970;53(2): 540–543.
62. Peng J, Jing F, Li D, Wang L. Pressure and temperature dependence of shear modulus and yield strength for aluminum, copper, and tungsten under shock compression. *Journal of Applied Physics*. 2005;98: 013508.
63. Li W, Kou H, Zhang X, Ma J, Li J, Geng P, Wu X, Chen L, Fang D. Temperature-dependent elastic modulus model for metallic bulk materials. *Mechanics of Materials*. 2019;139: 103194.
64. Lozinskii MG. *High Temperature Metallography*. New York: Pergamon; 1961.

65. Chang YA, Himmel L. Temperature dependence of the elastic constants of Cu, Ag, and Au above room temperature. *Journal of Applied Physics*. 1966;37(9): 3567–3572.
66. Reed RP, Mikesell RP. Low temperature (295 to 4K) mechanical properties of selected copper alloys. *Journal of Materials*. 1967;2: 370–392.
67. Joshi D, Bhatnagar ML. Temperature dependence of Young's modulus of copper, silver and gold. *Indian Journal of Pure and Applied Physics*. 1970;8: 428–431.
68. Tikhonov LV, Kononenko GI. *Mechanical properties of metals and alloys*. Kiev; 1986. (In Russian)
69. Ciftci YO, Colakoglu K, Kazanc S, Ozgen S. The effect of pressure on the elastic constants of Cu, Ag and Au: a molecular dynamics study. *Central European Journal of Physics*. 2006;4(4): 472–480.
70. Yokoo M, Kawai N, Nakamura KG, Kondo K, Tange Y, Tsuchiya T. Ultrahigh-pressure scales for gold and platinum at pressures up to 550 GPa. *Physical Review B*. 2009;80(10): 104114.
71. Matsui M. High temperature and high pressure equation of state of gold. *Journal of Physics: Conference Series*. 2010;215(1): 012197.
72. Biswas SN, Van't Klooster P, Trappeniers NJ. Effect of pressure on the elastic constants of noble metals from –196 to +25°C and up to 2500 bar: II. Silver and gold. *Physica B+C*. 1981;103(2–3): 235–246.
73. Hiki Y, Granato AV. Anharmonicity in noble metals; Higher order elastic constants. *Physical Review*. 1966;144(2): 411–419.
74. Daniels WB, Smith CS. Pressure derivatives of the elastic constants of copper, silver, and gold to 10 000 bars. *Physical Review*. 1958;111(3): 713–721.
75. Song M, Yoneda A, Ito E. Ultrasonic measurements of single-crystal gold under hydrostatic pressures up to 8 GPa in a Kawai-type multi-anvil apparatus. *Chinese Scientific Bulletin*. 2007;52(12): 1600–1606.
76. Ledbetter HM, Naimon ER. Relationship between single-crystal and polycrystal elastic constants. *Journal of Applied Physics*. 1974;45(1): 66–69.
77. Smith CS, Burns JW. The elastic constants of Cu-4 percent Si. *Journal of Applied Physics*. 1953;24(1): 15–18.